

Automated Vessel Shadow Segmentation of Fovea-centred Spectral-domain Images from Multiple OCT Devices

Jing Wu^a, Bianca S. Gerendas^a, Sebastian M. Waldstein^a, Christian Simader^a and Ursula Schmidt-Erfurth^a

^aChristian Doppler Laboratory for Ophthalmic Image Analysis, Department of Ophthalmology and Optometry, Medical University of Vienna, Austria

ABSTRACT

Spectral-domain Optical Coherence Tomography (SD-OCT) is a non-invasive modality for acquiring high resolution, three-dimensional (3D) cross sectional volumetric images of the retina and the subretinal layers. SD-OCT also allows the detailed imaging of retinal pathology, aiding clinicians in the diagnosis of sight degrading diseases such as age-related macular degeneration (AMD) and glaucoma.¹ Disease diagnosis, assessment, and treatment requires a patient to undergo multiple OCT scans, possibly using different scanning devices, to accurately and precisely gauge disease activity, progression and treatment success. However, the use of OCT imaging devices from different vendors, combined with patient movement may result in poor scan spatial correlation, potentially leading to incorrect patient diagnosis or treatment analysis. Image registration can be used to precisely compare disease states by registering differing 3D scans to one another. In order to align 3D scans from different time-points and vendors using registration, landmarks are required, the most obvious being the retinal vasculature.

Presented here is a fully automated cross-vendor method to acquire retina vessel locations for OCT registration from fovea centred 3D SD-OCT scans based on vessel shadows. Noise filtered OCT scans are flattened based on vendor retinal layer segmentation, to extract the retinal pigment epithelium (RPE) layer of the retina. Voxel based layer profile analysis and k -means clustering is used to extract candidate vessel shadow regions from the RPE layer. In conjunction, the extracted RPE layers are combined to generate a projection image featuring all candidate vessel shadows. Image processing methods for vessel segmentation of the OCT constructed projection image are then applied to optimize the accuracy of OCT vessel shadow segmentation through the removal of false positive shadow regions such as those caused by exudates and cysts. Validation of segmented vessel shadows uses ground truth vessel shadow regions identified by expert graders at the Vienna Reading Center (VRC). The results presented here are intended to show the feasibility of this method for the accurate and precise extraction of suitable retinal vessel shadows from multiple vendor 3D SD-OCT scans for use in intra-vendor and cross-vendor 3D OCT registration, 2D fundus registration and actual retinal vessel segmentation. The resulting percentage of true vessel shadow segments to false positive segments identified by the proposed system compared to mean grader ground truth is 95%.

Keywords: automated vessel shadow segmentation, 3D OCT, retinal disease, multimodal registration, pathology removal, image processing

1. INTRODUCTION

Age-related macular degeneration (AMD), glaucoma and other sight threatening diseases can be imaged and identified using 3D spectral domain optical coherence tomography (SD-OCT) of the eye, providing high resolution 3D cross-sectional images of the retinal structure. OCT imaging of the eye can also be used to assess disease progression by allowing clinicians to track changes in retinal anatomical structures over time. An important image processing tool to track disease progression is registration of retinal structures across different OCT scans and scanners. However, accurate and precise landmarks are required, of which the retinal vasculature is an obvious choice due to the visibility and temporal consistency of the vessel tree across patients. However, the retinal vessels themselves are not clearly visible within all OCT scans or within individual slices. However the

Further author information: (Send correspondence to Jing Wu)

Jing Wu: E-mail: jing.a.wu@meduniwien.ac.at, Telephone: +43(0)14040073703

vessel shadows, generated as a result of light attenuation in OCT, can be used as vessel locators. This work proposes and evaluates a novel application of automated retinal vessel segmentation on fovea centred 3D OCT images featuring pathology.

The majority of work on 3D OCT vessel segmentation has focussed on segmentation of the vessel shadows in optic nerve head (ONH) centred images where vessel shadows appear considerably more prominent due to higher contrast.²⁻⁴ However, diseases that affect patients vision target the macula, where the images may appear highly deformed as a result. In addition to their presence in macula centred images, disease pathology can also affect the visibility of the vessels too. Current work on vessel segmentation focus primarily on a single vendor,^{2,5} whereas this work presents a method capable of accurately and precisely delineating the true vessel shadows from multiple vendor scans. Screening patients using multiple vendor scanners is beneficial due to the ability for different scanners to image different aspects of disease, described by Simader et al.⁶ with unpublished additional data.

2. METHODOLOGY

The presented automated method can be applied to multiple vendor scans including Nidek RS3000, Zeiss Cirrus and Topcon 3D OCT 2000. The major methodological steps presented here are outlined in the flowchart shown in Figure 1.

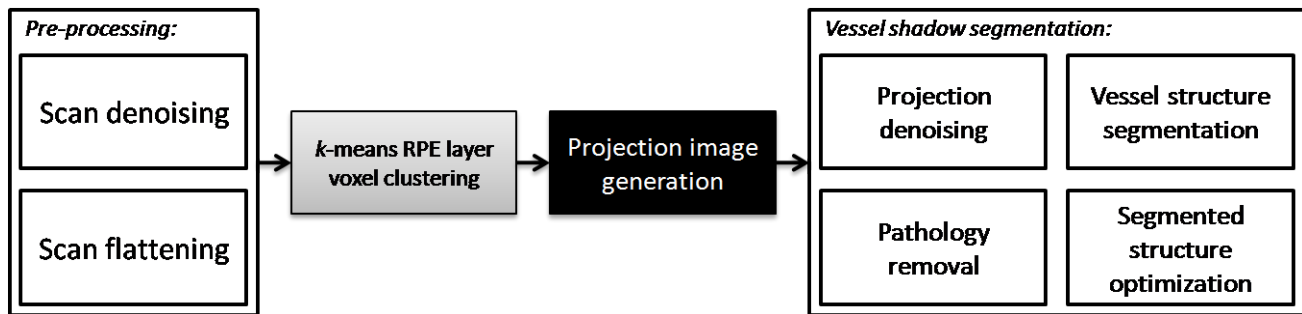


Figure 1. Flowchart outlining the major steps in this methodology.

2.1 Scan Pre-processing

2.1.1 Flattening

The voxels representing vessel shadows are most prominently seen in the retinal pigment epithelium (RPE) layer due to the contrast between the low intensity shadow voxels and the higher intensity layer tissue voxels. Thus it is necessary to isolate and extract this layer from the image slice in order to perform candidate vessel shadow segmentation. However the retina, as seen in OCT, is curved (Figure 2(a)), making the task of extracting the RPE layer challenging as it appears originally. Thus requiring the flattening of the retinal layers in the OCT image slice plane, also know as the XZ or B-scan.

Flattening, as demonstrated by Lee et al.,⁴ corrects every voxel within a B-scan such that the retinal layers are no longer curved. This is accomplished by performing voxel column shifting using the positional information of the lowest retinal surface (RPE) and the highest, the inner limiting membrane (ILM) surface obtained from the respective vendor layer segmentations. RPE flattening employs the lowest point on the vendor RPE surface segmentation as the base point. The distance between every other point along the RPE surface is calculated against the base point and the entire column of voxels is shifted accordingly such that the RPE surface is straight, as seen in Figure 2(b).

On the RPE flattened B-scan, the aforementioned base point is used to define the lower RPE boundary. The upper boundary of the RPE is defined as being 5 voxels above the lower RPE surface, based on dataset assessment, constructing a $5 \times N$ RPE layer matrix. Niemeijer et al.² describe averaging of the voxels within the

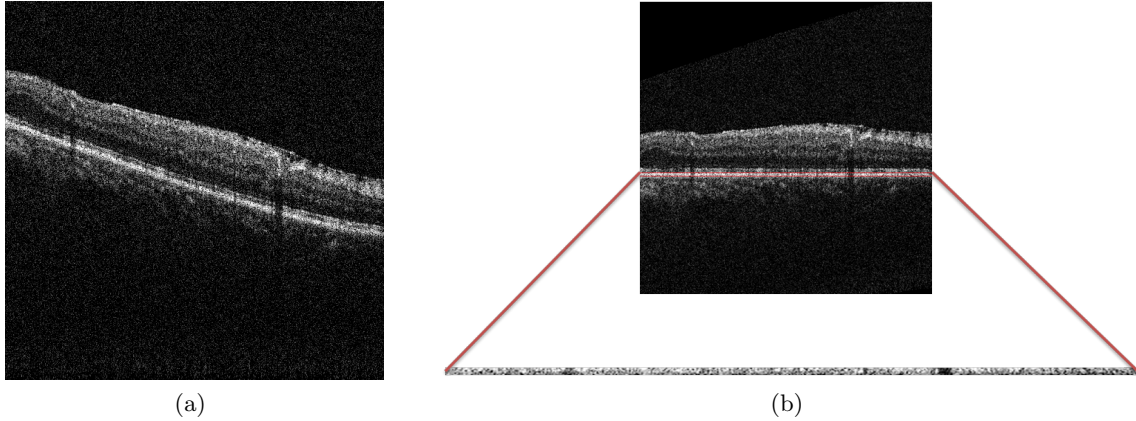


Figure 2. (a) Exempler OCT scan slice featuring curved retinal layers and (b) resulting flattened slice from (a) with the RPE layer boundaries highlighted in red.

RPE layer in the z direction to generate a line profile featuring candidate vessel shadows with enhanced contrast. This method has shown to be suitable for images featuring no or low levels of disease where only the retinal vessels produce the major shadows. However, the presence of pathology results in false positive shadows that may be confused with those of the vessels, thus both the averaged and original projection images are considered in this work. In addition, this method is not suitable for scans from vendors that acquire fewer B-scans resulting in a squashed projection image. Thus layer matrix averaging will only be used for scans with a larger number of B-scans.

2.1.2 Scan noise filtering

OCT scans feature varying levels of speckle noise depending on the vendor, as seen in Figure 3, caused by the attenuation of photons with the different organic matter in the eye. This leads to inconsistencies in object appearance as a result and specifically in the RPE layer, vessel shadow voxels may vary in intensity. The method employed in this work for denoising has been presented by Dabov et al.⁷ aiming to attenuate additive white gaussian noise from grayscale images through sparse transform-domain collaborative filtering. The suitability of this de-noising scheme has shown to perform optimally for OCT speckle noise reduction and the preservation of anatomical region boundaries.

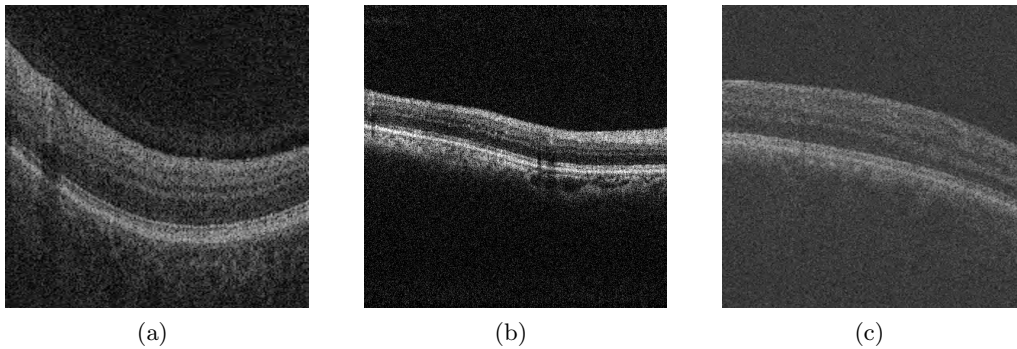


Figure 3. Exempler B-scans from vendors (a) Zeiss Cirrus, (b) Nidek RS3000 and (c) Topcon 3D OCT 2000 showing the variation in noise appearance in addition to retinal tissue appearance.

2.1.3 Candidate vessel shadow voxel clustering

K -means clustering is used to extract all the candidate vessel shadow voxels from the RPE layer matrices, an example of which can be seen in Figure 2(b), to distinguish them from background tissue. This method clusters together regions of like voxels that may represent the retinal vessel shadows. However, such a method may lead

to severe over-inclusion (in some cases doubling the number of candidate regions or more) due to the presence of false positive shadows caused by other pathology such as exudates, microaneurysms and fluid filled cysts. Thus in the next sections, a method of candidate vessel shadow voxel optimization is presented to remove false positive voxels.

2.2 Vessel shadow segmentation

Given the averaged and original RPE layer matrices for each OCT B-scan, a 2D projection image is created from the 3D volume, as seen in Figures 6. The projection image displays all the candidate vessel shadow voxels in the absence of a fundus image which may not always be available. From this projection image the vessel shadows are visible as connected, low intensity voxels featuring bifurcations and connected branches. From this projection image, the segmentation and extraction of the vessel shadows is carried out to optimize the voxel clustering result. The major steps involved in vessel segmentation are shown in the flowchart seen in Figure 2.2.

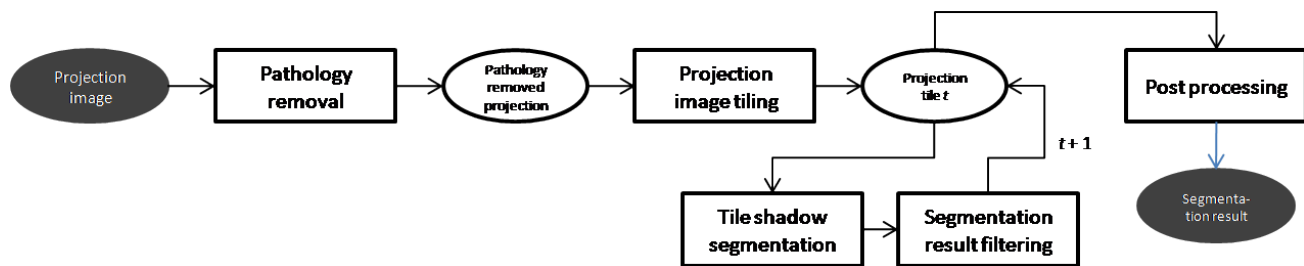


Figure 4. Flowchart outlining the major steps required for vessel shadow segmentation.

2.2.1 Projection noise reduction

The presence of speckle noise is a factor as the projection image has been constructed directly from the original OCT B-scans, seen as the varying grayscale specks in Figures 6(a), 6(c) and 6(e). In addition, given the difference in appearance between the vendors, the resulting projection images appear different and thus prove challenging for a global vessel shadow segmentation method. Firstly, noise filtering as mentioned previously is used to reduce the level of speckle noise, resulting in better vessel shadow contrast and clarity. Figure 6 shows example projection images from the 3 vendors assessed in this work in 6(a), 6(c) and 6(e) and the noise filtered result, where as an example $\sigma = 20$, in Figures 6(b), 6(d) and 6(f). Higher σ values result in stronger denoising, but will also reduce the clarity shadows, specifically smaller, less visible shadows.

2.2.2 Pathology shadow removal

In the following step, pathology found within the projection image needs to be removed to prevent it from interfering with or being mistaken for actual retinal vessel shadows. This step firstly examines the original projection image that has been converted to grayscale for all low intensity voxels below a threshold of 0.1 as shadows caused by pathology have an extremely low intensity. Region growing is employed using these identified points as seeds. However, this feature is shared by vessels and thus morphological thinning is used on all candidate detected regions, from which their perimeter and area are used to determine if they are long thin objects. If so, these are classed as vessels and removed from contention. Shadow regions that are identified as belonging to pathology are masked with voxel intensities randomly taken from the range of intensities that comprise the edge boundary of the respective pathology region. This ensures that the area of removed pathology blends with the neighbourhood background voxels.

The pathology removed projection image is tiled into sections of equal dimensions to reduce the segmentation operation, as shown in Figure 5. Multiple tile sizes are used including, 4×4 , 3×3 , 2×2 , 2×1 and 1×2 which ensure maximum coverage of the image.

Finally, for each tile a vessel enhancement filter as described by Frangi et al.⁸ is applied resulting in an initial delineation of the candidate vessel shadows. From the initial identified vessels, seed points are identified as the

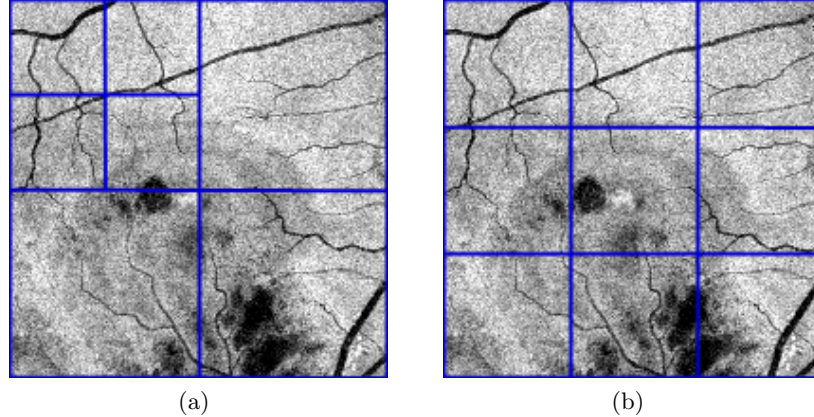


Figure 5. (a) Tiling patterns 4 x 4, 2 x 2, 2 x 1 and 1 x 2 and (b) tiling pattern 3 x 3 as described in Section 2.2.

highest intensity voxels and region growing is performed on the noise filtered projection image tile to extract the entire vessel shadow. This process is repeated on each of the tiles.

2.2.3 Vessel shadow segmentation optimization

The resulting segmented vessel shadows from each tile are compiled into the original projection image giving the locations of only true retinal vessel shadows. At which point this series of vessel regions is applied as a mask to the clustered candidate vessel shadow points described in Section 2.1.3. This allows the candidate vessel shadow voxels obtained from the original OCT B-scans to be filtered of non-vessel shadows.

3. MATERIALS

The data used in this work is comprised of 3D SD-OCT scans from 3 different vendor scanners. Each scan is comprised of contiguous B-scans that represent the layers of the retina perpendicular to the fundus plane. The data set has been obtained from patients suffering from exudative retinal diseases such as AMD, retinal vein occlusion and diabetic retinopathy with diabetic macular edema. Scans include both eyes, disease related pathology and are fovea centred, thus not featuring the ONH. Fovea centring was carried out by medical experts according to VRC guidelines for centre point re-plotting. OCT scan volume composition ranges from 128 to 256 slices with dimensions of 200 x 1024 to 512 x 512 voxels. 18 scans were assigned for training and 12 for testing.

Method validation employs ground truth OCT vessel shadow annotations by two expert graders. Grader annotation is performed using a proprietary system and is completely manual, relying on grader expertise only. The grader is tasked with assessing each OCT B-scan to identify the left and right boundary points for each vessel shadow from other shadows in the RPE layer. The annotation process is performed by each grader three times, with at least one week between the annotation of the same dataset in random order. Retention bias is not considered to be problematic due to the large volume of B-scans each grader is tasked with annotating. The final ground truth vessel shadows comprise the detected voxels between the graders across all annotation rounds correlated using logical conjunction.

The test set consists of 4 Cirrus, 4 Nidek and 4 Topcon scans. Aside from the differences in slice composition and dimensions, each scanner vendor will output scans with inter-vendor differences. This can include variations in intensity and clarity of physiology, introducing artefacts which, when coupled with the affects of motion and pathology, make distinguishing between vessel and non vessel shadows difficult. This is emphasized by the Sørensen-Dice coefficient (SDC) metric used to compare grader annotations between pairs of annotations rounds. Grader 1 annotated with an overall mean SDC of 0.734 compared to an overall mean SDC of 0.668 for Grader 2, giving an inter-grader mean SDC of 0.701.

The construction of the overall intra-observer ground truth comparison images (T_{Grader}) utilize the intersection of annotated vessel shadow voxels between pairs of annotation rounds (R_1, R_2, R_3) and the alternation between these pairs such that $T_{Grader} = (R_1 \cap R_2) \vee (R_2 \cap R_3) \vee (R_1 \cap R_3)$. The overall inter-observer ground

truth comparison images ($T_{Overall}$) are constructed from the intersection of T_{Grader_1} and T_{Grader_2} such that $T_{Overall} = T_{Grader_1} \cap T_{Grader_2}$.

4. RESULTS

The output from the vessel shadow segmentation method described here was compared with the ground truth vessel shadow locations as annotated by expert graders (Section 3). The primary comparison aims to assess the accuracy of the automated vessel shadow segmentation system and thus is sensitivity orientated, focussing primarily on true vessel shadows identified as such and false positive vessel shadows identified by the system. Validation is based on vessel shadow segment comparison where a vessel shadow segment is defined for the system output as a series of connected voxels comprising a candidate vessel shadow between bifurcations. Thus the system output would comprise true positive vessel shadow segments (TPSS) and false positive vessel shadow segments (FPSS).

When compared against the overall inter-observer ground truth ($T_{Overall}$), in 2 cases, no false positive vessel shadows were identified. This is similarly seen in comparison with Grader 2 (T_{Grader_2}) but increases to 6 cases when in comparison with Grader 1 (T_{Grader_1}). The mean percentage of true positive to false positive vessel shadow segments identified by the system when examined against the inter-observer ground truth is 81%, rising to 88% when compared against Grader 1 and 84% when compared against Grader 2. In cases 9,10 & 12, the higher number of false positive vessel shadow segments identified by the system is attributed to the presence of severe artefacting likely related to motion or their specific scanning protocol, as seen in Figure 6(e) & 6(f). Taking this into consideration, the mean percentage of true positive to false positive vessel shadow segments for inter-observer ground truth validation becomes 90%, rising to 97% for Grader 1 and 93% for Grader 2 intra-observer comparison.

A high percentage of true positive vessel shadow segments over false positive vessel shadow segments implies that our automated system is able to focus detection of the shadows which represent the retinal vessels with minimal to no confusion with shadows as a result of non-vessel constructs such as pathology.

5. CONCLUSIONS AND FURTHER WORK

An automated method for retinal vessel shadow segmentation of Fovea-centred SD-OCT images has been presented which is applicable to multiple OCT vendor devices. The results show that the method presented performs well across multiple vendor images and is capable of handling varying degrees of disease severity caused by cysts and exudates. This was aided by the pathology detection and removal stage within the projection image to prevent shadows generated by pathology from interfering or being confused for true vessel shadows.

Although the results of the system are generally good, some issues remain. Cases of poor performance were caused by artefacts such as noise, unfiltered by the system, and motion. As OCT images are generally very noisy, denoising is a very important stage. However, the removal of noise must be balanced with the retention of image detail, specifically the smallest and least visible vessel shadows. In addition, artefacts resulting from motion may lead to poor clarity in the projection image and the presence of unwanted noise, leading to incorrect identification or rejection of vessel shadows. In future work we hope to apply motion correction to OCT volumes in order to reduce or remove many motion related artefacts. Combined with improved denoising which maintains the consistency of smaller vessel shadows in both the B-scan and projection image, it is believed that smaller vessel shadows can be identified with greater accuracy, leading to a greater number of bifurcations. However, the method presented has shown to be capable of extracting the larger vessel shadows and many smaller ones in addition, thus allowing the identification of suitable bifurcations for use in other areas such as registration.

Further work aims to automatically extract suitable feature points from the segmented OCT vessel shadows for use in spatio-temporal 3D OCT registration. Likely landmark points will be major vessel and bifurcations due to their consistent presence. In addition to this is the generation of an accurate 3D model of the segmented vessels based on the geometric properties obtainable from the vessel shadows.

In summary, an automatic method for extraction of the retinal vessel shadows from multiple vendor, fovea-centred SD-OCT scans has been presented. This method has allowed the extraction of the locations of retinal

vessels from around the fovea which is highly affected by pathology in patients suffering sight degrading diseases such as AMD and glaucoma, which can be used for further analysis of the vessels and related diseases or as landmarks in OCT registration.

ACKNOWLEDGEMENT

The financial support of the Austrian Federal Ministry of Economy, Family and Youth and the National Foundation for Research, Technology and Development is gratefully acknowledged.

REFERENCES

1. Geitzenauer, W., Hitzenberger, C. K., and Schmidt-Erfurth, U. M., “Retinal optical coherence tomography: past, present and future perspectives,” *Br J Ophthalmol* **95**, 171–7 (July 2010).
2. Niemeijer, M., Garvin, M. K., van Ginneken, B., and Abràmoff, M. D., “Vessel segmentation in 3d spectral oct scans of the retina,” in [*Proceedings of the SPIE Medical Imaging*], **6914** (March 2008).
3. Hu, Z., Niemeijer, M., Abràmoff, M. D., Lee, K., and Garvin, M. K., “Automated segmentation of 3-d spectral oct retinal blood vessels by neural canal opening false positive suppression,” in [*Med Image Comput Comput Assist Interv.*], 33–40 (2010).
4. Lee, K., Abràmoff, M. D., Niemeijer, M., Garvin, M. K., and Sonka, S., “3-d segmentation of retinal blood vessels in spectral-domain oct volumes of the optic nerve head,” in [*Proceedings of the SPIE Medical Imaging*], **7626** (March 2010).
5. Pilch, M., Wenner, Y., Strohmayr, E., Preising, M., Friedburg, C., zu Bexten, E. M., Lorenz, B., and Stieger, K., “Automated segmentation of retinal blood vessels in spectral domain optical coherence tomography scans,” *Biomedical Optics Express* **3**, 1478–91 (July 2012).
6. Simader, C., Montuoro, M., Waldstein, S., Gerendas, B., Lammer, J., Heiling, U., Kuni, M., and Schmidt-Erfurth, U., “Retinal thickness measurements with spectral domain optical coherence devices from different manufacturers in a reading center environment,” in [*Proceedings of ARVO*], (2012).
7. Dabov, K., Foi, A., Katkovnik, V., and Egiazarian, K., “Image denoising by sparse 3d transform-domain collaborative filtering,” *IEEE Transactions on Image Processing* **16** (August 2007).
8. Frangi, A., Niessen, W. J., Vincken, K. L., and Viergever, M. A., “Multiscale vessel enhancement filtering,” *MICCAI* **1496**, 130–37 (1998).

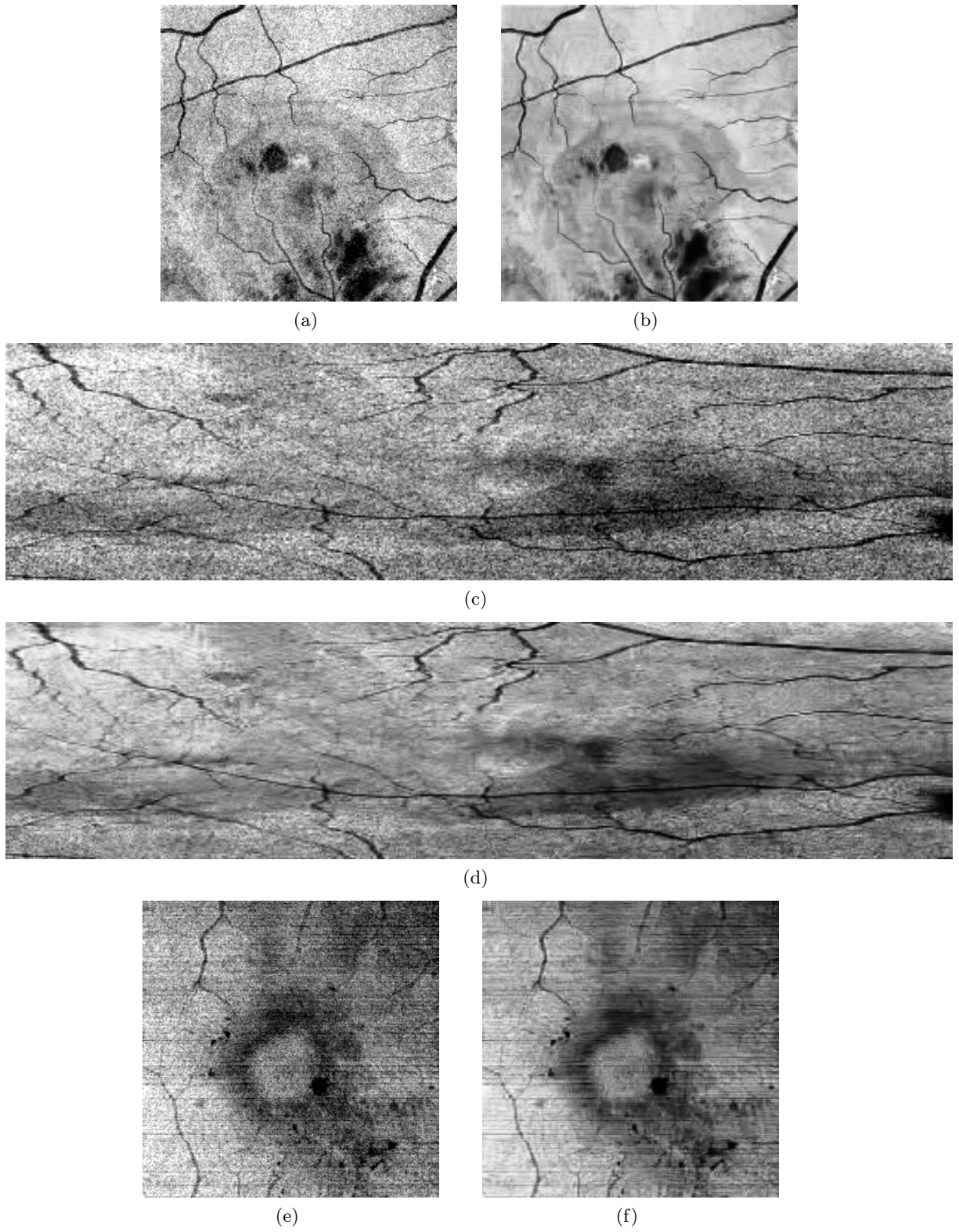


Figure 6. (a) Exemplar projection image of a Cirrus scan, (b) the result of noise filtering as described by Dabov et al.⁷ with $\sigma = 20$, (c) exemplar Nidek projection image, (d) noise filtered (c), (e) exemplar Topcon projection image and (f) noise filtered (e).